Applied Catalysis A: General 525 (2016) 145–157

Contents lists available at ScienceDirect

Applied Catalysis A: General

journal homepage: www.elsevier.com/locate/apcata

Influence of pretreatment atmospheres on the performance of bimetallic Au-Pd supported on ceria-zirconia mixed oxide catalysts for benzyl alcohol oxidation

Carol M. Olmos[a], Lidia E. Chinchilla[a], Alberto Villa[b], Juan J. Delgado[a], Huiyan Pan[a], Ana B. Hungría[a], Ginesa Blanco[a], Jose J. Calvino[a], Laura Prati[b], Xiaowei Chen (Dr.)[a,*]

[a] Departamento de Ciencia de los Materiales, Ingeniería Metalúrgica y Química Inorgánica, Facultad de Ciencias, Universidad de Cádiz, Campus Río San Pedro, Puerto Real, Cádiz E-11510, Spain
[b] Dipartimento di Chimica, Università deli Studi di Milano, Milano I-20133, Italy

ARTICLE INFO

Article history:
Received 23 May 2016
Received in revised form 7 July 2016
Accepted 18 July 2016
Available online 19 July 2016

Keywords:
Selective oxidation of benzyl alcohol
Bimetallic catalyst
Au
Pd
Ceria-zirconia
Thermal treatment

ABSTRACT

Monometallic Au, Pd and bimetallic Au-Pd catalysts supported on a $Ce_{0.62}Zr_{0.38}O_2$ mixed oxide have been synthesized by the sol-immobilization method. An in-depth Scanning-Transmission Electron Microscopy (STEM) study has been performed to reveal the structural and chemical nature of the metal nanoparticle system present in these catalysts. Attention has been paid both to the evolution of the particle size distribution and the degree of Au-Pd interaction as a function of the treatment used to activate the catalysts. This characterization work has been complemented by results coming from other macroscopic techniques like Inductively Coupled Plasma-Atomic Emission Spectroscopy (ICP-AES), N_2 physisorption, Temperature Programmed Oxidation (TPO) or X-ray Photoelectron Spectroscopy (XPS). The whole set of characterization data evidences the intrinsic structural complexity of this type of bimetallic systems, in which a fraction of monometallic Au, monometallic Pd and bimetallic nanoparticles of varying compositions coexist. This picture, which clearly contrasts with other much more homogeneous situations described in previous literature on bimetallic catalysts, also indicates the requirement of combining both atomic scale and macroscopic techniques to understand the structure of these catalysts.

Concerning catalytic performance, a synergistic effect between Au and Pd has been observed in the selective oxidation of benzyl alcohol on ceria-zirconia. Moreover, the catalytic activity of these bimetallic Au-Pd catalysts is higher than that on other commonly used supports, such as activated carbon or carbon nanotubes. The treatments in oxidative and inert atmospheres at 250 °C improve the catalytic activity with respect to the fresh, un-pretreated, catalyst. Subsequent reduction of the oxidized bimetallic catalyst leads to an activity similar to that of the fresh catalyst, which is reduced at room temperature with H_2 bubbles.

1. Introduction

Benzaldehyde is one of the most valuable aromatic aldehydes due to its application in perfumery, pharmaceuticals, cosmetics, dyestuff and agrochemical industry. Commercially, it is mainly produced via the toluene chlorination/hydrolysis process, which generates large amounts of toxic acidic waste, leading to equipment corrosion and costly separation processes [1]. The high demand for green processes and in particular, the need for chlorine-free benzaldehyde production has promoted the development of novel, environmental benign and alternative production routes.

Selective oxidation of benzyl alcohol to benzaldehyde in liquid phase has shown advantages in terms of easy recovery, reusability and high catalytic activity [1]. Among heterogeneous catalysts, bimetallic catalysts integrating Au with other noble metals (Pd and Pt) have exhibited higher catalytic activity than monometallic catalysts for the selective oxidation of benzyl alcohol [2–11]. In particular, Au-Pd nanoparticles supported on different kinds of supports have demonstrated promising results [2–11].

Even though selective oxidation of benzyl alcohol on Au-Pd catalysts is a well-studied process in the literature, the detailed nature of the interaction between the two metals at atomic level has not

* Corresponding author.
E-mail address: xiaowei.chen@uca.es (X. Chen).

http://dx.doi.org/10.1016/j.apcata.2016.07.013
0926-860X/

been considered in full details, in spite of its relevance to understand their performance. Recent reports on gold-based bimetallic catalysts, prepared by different approaches have pointed out that a complex nanostructure in this kind of materials forms [12,13].

On the other hand, the support plays an important role in the oxidation of benzyl alcohol. Thus, bimetallic Au and Pd nanoparticles have been deposited on different kinds of materials, such as activated carbon, carbon nanotubes, TiO_2, Mg-Al mixed oxide, ceria, ZnO, Nb_2O_5, SiO_2, Al_2O_3, SBA-15, zirconia, polyaniline or MgO, among others [2–11,14–25]. It has been reported that gold and palladium nanoparticles supported on reducible oxides, such as CeO_2, exhibit better catalytic behavior due to the ability of these materials to activate the O_2 molecule [14,26]. In particular, CeO_2 is a very reactive support due to its unique redox properties, related to its capacity to reversibly exchange lattice oxygen with its surroundings in response to changes in the oxidation state of cerium atoms between Ce^{4+} and Ce^{3+}, which is usually referred as oxygen storage capacity (OSC). Furthermore, the introduction of Zr^{4+} ions into the CeO_2 fluorite lattice improves the OSC, the formation of oxygen vacancies [27] and the thermal stability with respect to the pure oxide [28,29]. Only a few works have studied ceria-zirconia mixed oxides as supports for bimetallic Au-Pd catalysts. A previous contribution from our lab has reported that no synergistic effect was found on bimetallic Au-Pd catalysts supported on ceria-zirconia prepared by deposition-precipitation (DP) of Au followed by impregnation of Pd method for CO oxidation reaction [30]. In contrast, synergistic effects were observed on both bimetallic Au-Pd and Au-Ru supported on ceria-zirconia mixed oxide catalysts for selective oxidation of glycerol [12,31].

Taking all this into consideration, in this work, bimetallic Au-Pd catalysts supported on a $Ce_{0.62}Zr_{0.38}O_2$ oxide have been prepared by sol-immobilization method and a detailed characterization work has been performed in order to determine the extent of Au-Pd interaction reached using this particular type of synthetic approach. Their catalytic performance in the selective oxidation of benzyl alcohol has been evaluated. In particular, the effect of the redox nature of the activation pretreatment atmosphere has been studied in order to optimize the synthesis method of bimetallic Au-Pd catalysts supported on $Ce_{0.62}Zr_{0.38}O_2$. Thus, pretreatments under hydrogen, nitrogen and oxygen have been investigated as representative of activation of the catalysts under reducing, inert and oxidizing conditions.

2. Experimental

2.1. Catalyst preparation

The support used in all the preparations described below was a $Ce_{0.62}Zr_{0.38}O_2$ (CZ) mixed oxide kindly donated by Grace Davison. The BET surface area of this commercial material was 67 $m^2\,g^{-1}$.

2.1.1. Monometallic catalysts

The monometallic and bimetallic catalysts have been prepared by the sol-immobilization method. The nominal loadings of the monometallic catalysts were 1 wt.%. 2 mL of Na_2PdCl_4 (10 mg Pd mL^{-1}) solution and 2 mL of polyvinylpyrrolidone aqueous solution (PVP, 1%, w/w) were added to 200 mL of deionized water, stirring for 2 min. Then 4 mL of 0.1 M $NaBH_4$ solution was put into the mixture of the Pd precursor and PVP under magnetic stirring for sol generation. A brown Pd sol immediately formed. An UV–vis spectrum of the Pd sol was recorded for ensuring the complete reduction of Pd(II).

The Au sol was prepared with the same method using $NaAuCl_4{\cdot}2H_2O$ as precursor. A ruby red Au sol immediately formed after addition of $NaBH_4$ solution to the mixture of $NaAuCl_4$ and PVP. The UV–vis spectrum of the gold sol also confirmed complete reduction of Au (III) species.

Within 3 min from their generation, the colloids (acidified to pH = 2 by addition of sulfuric acid) were immobilized by adding 2 g of $Ce_{0.62}Zr_{0.38}O_2$ mixed oxide support under vigorous stirring for 1 h. The slurry was further filtered, washed with distilled water and dried at 80 °C for 2 h. The dried catalysts were oxidized in a flow of O_2 for 1 h at 250 °C with a heating rate of 10 °C min^{-1}. Then, the treatment atmosphere was changed at the same temperature to a flow of nitrogen. After 1 h under this environment, the catalyst was cooled down to room temperature, also under the nitrogen flow. The monometallic catalysts were coded as 0.82%PdCZ and 0.86%AuCZ, in which 0.82% and 0.86% stand for the actual Pd and Au loadings as determined from ICP-AES analysis.

Another monometallic reference 2.5 wt.% $Au/Ce_{0.62}Zr_{0.38}O_2$ catalyst was prepared by DP method using sodium carbonate as precipitating agent [12,30]. This DP sample was filtered and washed several times with deionized water at room temperature until no chloride ions could be detected with $AgNO_3$. It was dried overnight in an oven at 100 °C. Finally the sample was oxidized at 250 °C in 5% O_2/He for 1 h and purged with a flow of helium at the same temperature for 1 h. Cooling down to room temperatures was also performed under the inert gas flow. This catalyst is coded as 2.5%AuCZ. As described in our previous work [12,30], the size of the Au metal particles of this 2.5%AuCZ catalyst ranges from 1 to 8 nm, with an average value of 1.7 nm. The metal dispersion of this catalyst is 39%.

2.1.2. Bimetallic Au-Pd catalysts

In order to synthesize bimetallic Au-Pd supported on ceria-zirconia catalysts with total metal loading around 1 wt.%, a Au sol was firstly prepared using the same method described for the 0.86%AuCZ catalyst. 2.19 mL of $NaAuCl_4{\cdot}2H_2O$ (10 mg Au mL^{-1}) solution and 2.19 mL PVP solution (1%, w/w) were added in 219 mL of H_2O. After stirring for 2 min, 0.1 M $NaBH_4$ (4.38 mL) was added under vigorous magnetic stirring. The ruby red Au sol immediately formed. After 3 min of sol generation, 3 g of $Ce_{0.62}Zr_{0.38}O_2$ support was added to the Au sol under vigorous stirring. After 1 h of stirring, the slurry was filtered and washed with distilled water and dried during 15 min at 80 °C.

The second step of the preparation was deposition of Pd on the $Au/Ce_{0.62}Zr_{0.38}O_2$ sample. For this purpose, the monometallic Au sample previously prepared was dispersed in 250 mL of water at room temperature. To guarantee saturation, H_2 was bubbled for 1 h (50 mL min^{-1}) into the suspension under atmospheric pressure and room temperature. Then, 0.81 mL of Na_2PdCl_4 (10 mg Pd mL^{-1}) solution and 0.81 mL of PVP solution (1%, w/w) were added under vigorous magnetic stirring. After additional 1 h of stirring, the resulting slurry was filtered and washed with distilled water and dried in air at 80 °C for 2 h. The catalyst obtained this way was coded as 1.4AuPd-F. Subsequently the 1.4AuPd-F catalyst was activated using three different pretreatments: (1) under nitrogen at 250 °C for 2 h (1.4AuPd-I); (2) under oxygen for 1 h followed by nitrogen 1 h also at 250 °C (1.4AuPd-O); (3) a portion of the 1.4AuPd-O sample was reduced bubbling H_2 at room temperature into a vigorously stirred aqueous suspension of this catalyst during 1 h (1.4AuPd-R).

2.2. Catalyst characterization

The gold and palladium loadings of the catalysts were determined by ICP-AES. X-ray diffraction (XRD) patterns of the catalysts were recorded using a Bruker diffractometer AXS, Model D8 Advance, employing Cu Kα radiation source (1.5418 Å) operated at 40 kV and 40 mA. Scans were collected from 10 to 100 ° with a 0.05 ° step size and step time of 30 s. The BET specific surface areas

of the catalysts were measured by adsorption of nitrogen at −196 °C on a Micromeritics ASAP-2020 instrument.

TPO profiles were registered using 100 mg of the catalyst placed in a U-Shaped quartz reactor. The outlet of the reactor was connected to a Pfeiffer Thermostar quadrupole mass spectrometer. The catalyst was heated from room temperature up to 900 °C with a heating rate of 10 °C min^{-1} in a flow of 5% O_2/He (60 mL min^{-1}).

STEM experiments were performed on a JEOL2010 field emission gun instrument equipped with an XEDS spectrometer Oxford INCA Energy 2000 system. HAADF-STEM images, whose intensity is roughly proportional to the square of the atomic number Z^2, were recorded by using an electron probe of 0.5 nm of diameter at a diffraction camera length of 8 cm. Based on the HAADF-STEM images of the Au-containing catalysts, metal particle diameters of more than 200 randomly selected metal particles were measured and corresponding metal particle size distributions were established (PSDs). From these PSDs, the average particle diameter (d) was determined according to the following expression: $d = \sum n_i d_i / \sum n_i$, where $n_i \geq 200$. The total metal dispersion was calculated according to $D = N_s/N_t$, where N_s and N_t are total number of surface metal atoms and total number of atoms in the whole PSD, respectively. The average particle size, metal particle size distribution and metal dispersion data have been calculated using a truncated cuboctahedron particle model [32] and a home-made software (GAUSS). More than 40 individual particles were analyzed in each bimetallic sample using STEM-XEDS technique. Quantification of the experimental STEM-XEDS spectra provided compositional information from each analyzed particle. Samples for STEM studies were prepared by depositing a small amount of the catalyst powder onto a holey carbon coated Cu grids. The use of any solvent was avoided.

XPS analyses were performed on a Kratos Axis Ultra DLD instrument. Spectra were recorded using monochromatized Al Kα radiation (1486.6 eV), with an X-ray power of 150 W. The spectrometer was operated in the Constant Analyzer Energy mode, with pass energy of 160 eV for low resolution and wide range survey spectra, and 20 eV for high resolution and narrow core level spectra. Powder samples were pressed into pellets, which were stuck on a double-sided adhesive conducting polymer tape. Surface charging effects were compensated making use of the Kratos coaxial neutralization system. The binding energy scale was calibrated with respect to the Zr $3d_{5/2}$ component of the mixed oxide support, and fixed at 182.64 eV as reported in our previous work [33]. XPS data analysis was performed with CasaXPS Software, version 2.3.17dev6.3a, developed by Neal Fairley (Casa Software Ltd, 2013).

2.3. Catalytic activity for benzyl alcohol oxidation

Catalytic tests were carried out in a thermally controlled glass reactor (30 mL) equipped with an electronically controlled magnetic stirrer connected to a large reservoir (5000 mL) containing oxygen [6]. The oxygen uptake was followed by a mass-flow controller. Benzyl alcohol and the catalyst (alcohol:total metal = 3000 mol:mol) were mixed in cyclohexane (benzyl alcohol:cyclohexane 50:50 (vol:vol); total volume: 10 mL). The reactor was pressurized at 200 kPa of oxygen and heated to 80 °C. The reaction was initiated by stirring and periodic removal of samples from the reactor was performed. Identification and quantification of the products were done by comparison with the external standard calibrated samples by a HP 7820A gas chromatograph equipped with a capillary column (HP-5 30 m 0.32 mm, 0.25 μm Film, made by Agilent Technologies) and thermal conductivity detector.

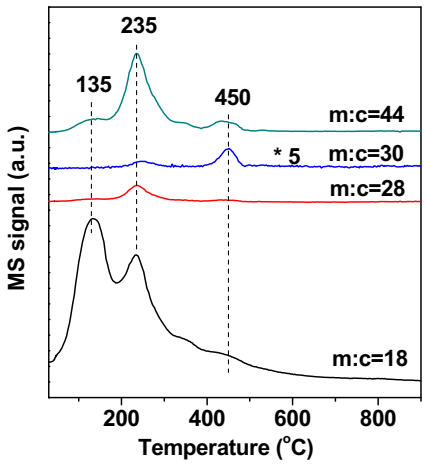

Fig. 1. Temperature programmed oxidation profiles of 1.4AuPd-F catalyst.

3. Results

During the synthesis, PVP was used to prepare Au and Pd sols. In order to determine the oxidation temperature required to remove this protecting agent from the surface of the catalysts, a TPO was performed over the fresh and dried 1.4AuPd-F catalyst (Fig. 1). The profiles of the mass:charge ratios of 28 and 44, corresponding to N_2 (or CO) and N_2O (or CO_2) species, indicate that these species evolve from the catalyst and reach their maxima at 135, 235 and 450 °C, respectively. The dominant peak for these two signals appears at 235 °C. The formation and desorption of N_2 (or CO) and N_2O (or CO_2) species suggest the decomposition of the protecting agent PVP. The mass:charge ratio 18, which can be assigned to H_2O, also depicts peaks at 135, 235 and 450 °C. However the strongest peak of H_2O appears around 135 °C. The mass:charge ratio of 30, which could be NO produced by decomposition of PVP, presents only two peaks: one is around at 235 °C; another is stronger at 450 °C. Since previous reports in the literature indicated that Au particles agglomerated when the pretreatment temperatures are higher than 400 °C [34,35] and our TPO results show that most of the signals of mass:charge ratios 18, 28, 30 and 44 can be removed at 250 °C. The monometallic 0.86%AuCZ and 0.82%PdCZ and bimetallic 1.4AuPd-F catalysts were pretreated with an oxidation at 250 °C to remove PVP and avoid strong sintering of Au and Pd.

3.1. Textural and structural properties

The textural properties of the different catalysts are listed in Table 1. The BET specific surface areas of the monometallic and bimetallic catalysts are in the range from 64 to 67 m^2g^{-1}, which are very close to that of the support. This result indicates that the treatments at 250 °C in oxidizing, inert atmospheres or after the further reduction at room temperature of the catalyst treated under oxygen do not induce any significant change in the surface areas of the catalysts.

The total theoretical Au and Pd loadings of the monometallic and bimetallic Au-Pd catalysts are 1 wt.%. However, elemental analyses show that the actual Au and Pd loadings are lower than the expected values, suggesting that this method does not lead to a complete deposition of Au and Pd on the $Ce_{0.62}Zr_{0.38}O_2$ support during the sol-immobilization synthesis. This fact might be due to the presence in the sols of a fraction of Au and Pd particles weakly bonded to the support surface that would be eventually removed during the filtering and washing steps.

XRD patterns of monometallic 0.86%AuCZ, 0.82%PdCZ and bimetallic catalysts pretreated under different atmospheres are

Table 1
Physico-chemical properties of the monometallic and bimetallic catalysts.

Catalyst	Pretreatment conditions	Au loading (wt%)		Pd loading (wt%)		Theoretical Au:Pd molar ratio	Actual Au:Pd molar ratio[b]	Au content (mol%)	S_{BET} (m^2g^{-1})	Average particle size (nm)[c]	Metal dispersion (%)[c]	Conversion (%)[d]	TOF (h^{-1})[e]
		Theoretical	Actual[a]	Theoretical	Actual[a]								
2.5%AuCZ	Oxidation at 250 °C	3.0	2.5	–	–	–	–	100	64	1.7 ± 0.1	39	3	162
0.86%AuCZ	Oxidation at 250 °C	1.0	0.86	–	–	–	–	100	67	6.0 ± 0.2	20	3	132
1.4AuPd-F	Dried at 80 °C	0.73	0.55	0.27	0.21	1.5	1.4	58	67	2.6 ± 0.1	43	77	805
1.4AuPd-O	Oxidation at 250 °C	0.73	0.55	0.27	0.21	1.5	1.4	58	66	3.5 ± 0.1	29	97	2260
1.4AuPd-I	Treated at 250 °C with N_2	0.73	0.55	0.27	0.21	1.5	1.4	58	66	3.9 ± 0.1	31	98	1775
1.4AuPd-R	1.4AuPd-O reduced at 25 °C with H_2	0.73	0.55	0.27	0.21	1.5	1.4	58	–	3.0 ± 0.1	37	91	1036
0.82%PdCZ	Oxidation at 250 °C	–	–	1.0	0.82	–	–	0	66	2.7 ± 0.1	37	87	302

[a] Weight percentage per gram of sample, obtained by ICP-AES analysis.
[b] Molar ratio was calculated by weight percentage of metal as determined by ICP-AES.
[c] The average particle size and metal dispersion were determined by STEM technique.
[d] Conversion at 2 h of reaction.
[e] TOF at 0.5 h of reaction.

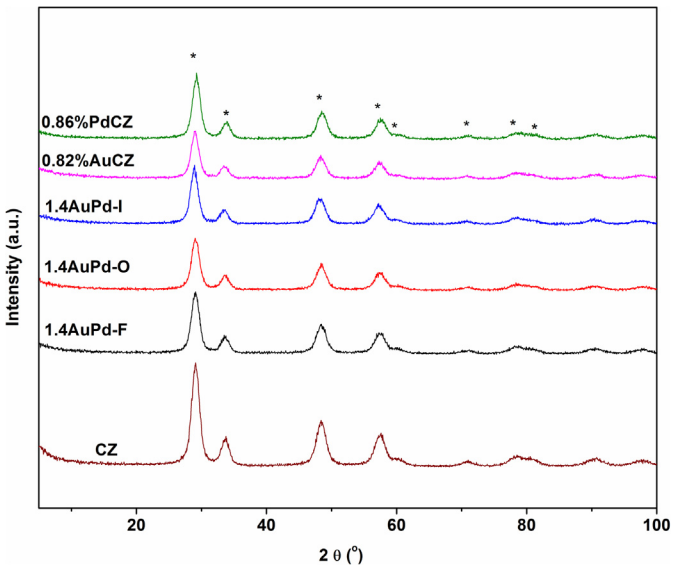

Fig. 2. XRD patterns of monometallic and bimetallic 1.4AuPd-F, 1.4AuPd-O and 1.4AuPd-I catalysts. * Diffraction of fluorite structure for $Ce_{0.62}Zr_{0.38}O_2$ mixed oxide.

shown in Fig. 2. The diffraction peaks at 2θ values of 29.0, 33.5, 48.2, 57.5, 60.3, 70.8, 77.0 and 80.9° correspond to the crystallographic planes {111}, {200}, {220}, {311}, {222}, {400}, {331} and {420} of the fluorite-type structure of ceria-zirconia mixed oxide [29–31]. Comparison between the XRD patterns of these catalysts suggests that the treatments at 80 °C or 250 °C under oxidizing or inert atmospheres do not generate any structural transformation in the ceria-zirconia mixed oxide. No peaks related either to Pd, Au, PdO or Au-Pd alloy phases could be detected in any catalyst, which reveals that the metal phases are well-dispersed, in the form of very small nanoparticles [12,30].

3.2. Catalytic activity for benzyl alcohol oxidation

The bimetallic catalysts activated under different conditions as well as the monometallic catalysts were evaluated for benzyl alcohol oxidation. Fig. 3 shows conversion of benzyl alcohol and the selectivity versus the reaction time over the catalysts. The 0.86%AuCZ catalyst prepared by sol-immobilization method reaches only 3% of conversion. Fig. 3 also depicts the catalytic activity results obtained on the second reference monometallic 2.5%AuCZ catalyst with higher Au loading and smaller particle size. Note that also in this case the activity is still quite low. In fact, a maximum benzyl alcohol conversion of 5% is reached after a total reaction time of 2 h. Neither the 0.86%AuCZ nor the 2.5%AuCZ catalyst has the ability to initiate the benzyl alcohol oxidation, even after a 2 h period. The rate-determining step for Au catalyst is alcohol oxidative dehydrogenation and the H-abstraction cannot occur on Au catalysts [36]. In clear contrast, the 0.82%PdCZ catalyst shows a drastic increase of conversion from 7% to 87% within the reaction time period between 1 and 2 h which the catalytic activity is higher than those of two monometallic Au catalysts. This result is in agreement with those reported in the literature [3,4,6]. The 1 h long induction period must be very likely related to a progressive removal of remnant PVP moieties attached to the surface of the Pd nanoparticles even after the oxidation at 250 °C. Note that in this respect TPO results show that the evolution of decomposition products is not totally completed at this temperature.

The comparison between the catalytic activities obtained from monometallic and bimetallic catalysts shows that the 1.4AuPd-O catalyst presents higher catalytic activity than the corresponding monometallic catalysts. This fact confirms the synergistic effect

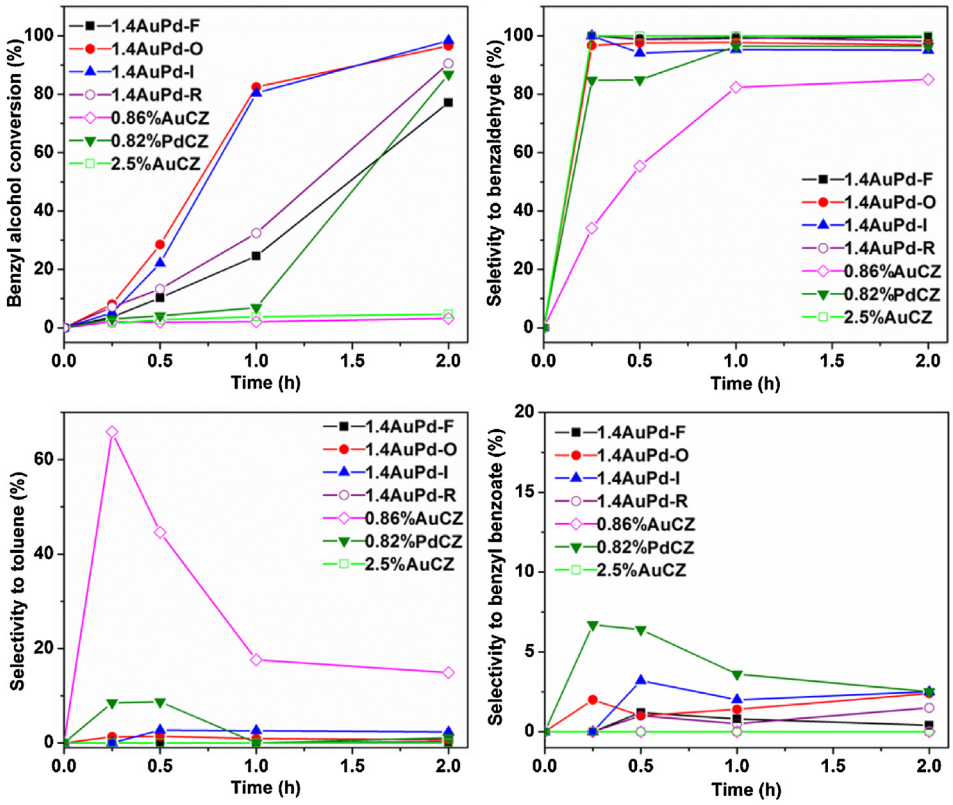

Fig. 3. Catalytic activities of benzyl alcohol oxidation in liquid phase as a function of time in the presence of the monometallic or bimetallic catalysts. Reaction conditions: alcohol:total metal ratio = 3000 mol:mol, benzyl alcohol:cyclohexane ratio = 50:50 vol:vol, reaction temperature: 80 °C. The reactor was pressurized at 200 kPa of oxygen.

Table 2
Comparison of benzyl alcohol oxidation data on the bimetallic Au-Pd catalysts.

Catalyst	Composition of the catalysts			TOF(h^{-1})	Conversion(%)	Selectivity (%)			Reference
	Au loading(wt%)	Pd loading(wt%)	Au:Pd molar ratios			Benzaldehyde	Benzyl benzoate	Toluene	
1.4AuPd-O	0.55	0.21	1.4	2260[a]	97 [b]	96	2	1	This work
1.4AuPd-I	0.55	0.21	1.4	1775[a]	98 [b]	95	2	2	This work
1%AuPd/AC	0.73	0.27	1.5	1350	90	89	–	9	[38]
1%AuPd/CNTs	0.73	0.27	1.5	1490	98	89	6	3	[38]

Reaction conditions, alcohol:metal molar ratio = 3000, T = 80 °C, pO_2 = 200 kPa, benzyl alcohol:cyclohexane ratio = 50:50.
[a] TOF at 0.5 h of reaction in this work.
[b] Conversion and selectivity at 2 h of reaction in this work.

between Au and Pd for benzyl alcohol oxidation already reported in the literature [6,8,14,22,37,38]. Moreover ceria-zirconia mixed oxide appears to promote the activity of Au-Pd catalyst. In fact, 1.4AuPd-O shows a TOF (2260 h^{-1}) higher than those of Au-Pd catalysts supported on other commonly used supports: activated carbon (1350 h^{-1}) and carbon nanotubes (1490 h^{-1}), as indicated in Table 2.

At 2 h of reaction time, the 1.4AuPd-O and 1.4AuPd-I catalysts show almost the same conversion, reaching a value around 97%, whereas the catalytic activity of the fresh 1.4AuPd-F catalyst is much lower. It is also important to mention that the maximum benzyl alcohol conversion is only 77% over the 1.4AuPd-F catalyst. On the other hand, the catalytic activity of the 1.4AuPd-R catalyst, obtained by reduction of 1.4AuPd-O using H_2 at room temperature, is only slightly higher than that of the fresh 1.4AuPd-F catalyst, which is also a reduced catalyst. TOF values at 0.5 h of reaction time are listed in Table 1. Among the bimetallic catalysts pretreated under different conditions, the TOF values follow the order: 1.4AuPd-O (2260 h^{-1}) > 1.4AuPd-I (1775 h^{-1}) > 1.4AuPd-R (1036 h^{-1}) > 1.4AuPd-F (805 h^{-1}).

In terms of selectivity, benzaldehyde is the main product (>95%) over the monometallic and bimetallic catalysts (Fig. 3), with a small amount of toluene (1–2%) and benzyl benzoate (2–3%) as byproducts. It is very important to stress at this point that the utilization of ceria-zirconia oxide as support has also a beneficial effect to limit the formation of the byproducts. Indeed, the 1.4AuPd-O catalyst shows a selectivity value to benzaldehyde of 96%, whereas using Au-Pd/AC and Au-Pd/CNTs a selectivity of only 89% was obtained, due to the 9% of undesired toluene and benzyl benzoate for AC support and 3% for CNTs support.

Recently Savara et al. proposed the reaction pathway for benzyl alcohol oxidation over Pd-containing catalysts shown as Scheme 1 [39]. According to these authors, benzyl alcohol is first oxidized to benzaldehyde via an alkoxy intermediate. This agrees well with the observed increase in selectivity to benzaldehyde during the first reaction period, which in this study reaches 85% on the 0.82%PdCZ catalyst and above 95% on the bimetallic catalysts. The selectivity to benzaldehyde reaches in fact at least 95% over all the Pd-containing catalysts when the reaction time is just of 1 h and remains stable at longer reaction time. Only a small amount of benzyl benzoate,

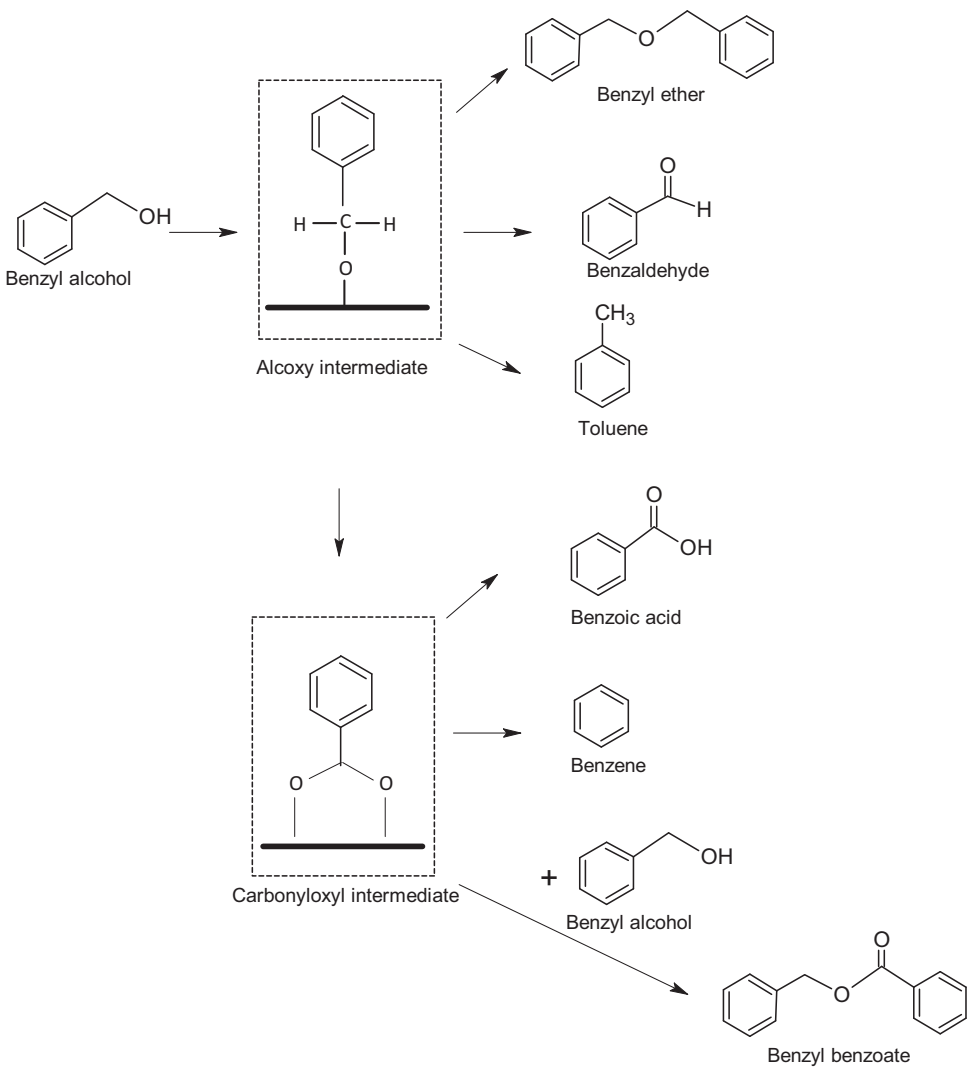

Scheme 1. Reaction pathways for benzyl alcohol oxidation [39].

deriving from benzaldehyde molecules that react with remaining benzyl alcohol, is formed as major byproduct (Scheme 1). On the bimetallic catalysts, the selectivity to benzyl benzoate is very low, less than 5%. Small amounts of toluene are also observed (Table 2). This byproduct is reported to be formed by the disproportionation of benzyl alcohol [40] or by the reaction of the intermediate metal hydride with the alcohol instead of O_2 [39,41]. No benzene is observed among the products, over neither the monometallic nor the bimetallic catalysts.

In summary, a synergistic effect has been observed to take place over the bimetallic Au-Pd catalysts supported on ceria-zirconia. Additionally, the ceria-zirconia promotes a significant increase of the selectivity to benzaldehyde as compared with other supports like activated carbon or carbon nanotubes. The bimetallic catalysts treated under oxidizing and inert atmospheres exhibit similar catalytic activities and similar selectivity toward benzaldehyde (>95%) with trace amounts of toluene and benzyl benzoate as byproducts, being more active and more selective to benzaldehyde than the fresh and reduced catalysts (1.4AuPd-F and 1.4AuPd-R).

3.3. STEM results

Fig. 4 shows representative STEM-HAADF images of the monometallic 0.86%AuCZ and 0.82%PdCZ reference catalysts. Note that in both cases the metal nanoparticles can be recognized from the image contrasts. The 0.82%PdCZ catalyst presents a narrow particle size distribution, with most of the particles ranging in diameter from 0.5 to 5 nm, while the 0.86%AuCZ catalyst shows a wider particle size distribution, from 1 to 12 nm. Correspondingly, the average particle sizes of the 0.82%PdCZ and the 0.86%AuCZ catalysts are 2.7 and 6.0 nm. As expected, the metal dispersion of 0.82%PdCZ catalyst (37%) is higher than that of 0.86%AuCZ catalyst (20%). On the other hand, the Au particle size of the 2.5%AuCZ catalyst is rather narrow and closer to that of the monometallic Pd catalyst, with all the particles within the 1–8 nm diameter range. In fact, the average particle size of this catalyst is 1.7 nm and the metal dispersion 39% [12,30].

Fig. 5 shows STEM-HAADF images and particle size distributions of the bimetallic catalysts activated under different atmospheres. The values of average particle size and metal dispersion of the bimetallic catalysts have been also listed in Table 1. These results indicate that thermal treatments in oxidizing and inert atmospheres at 250 °C lead to a slight growth of the particle size and a decrease of the metal dispersion. Hutchings et al. reported that the metal particle size of bimetallic Au-Pd supported on activated carbon and Al_2O_3 catalysts increased with increasing calcination temperature [42,43]. The reduction of 1.4AuPd-O at room temperature results only in a slight increase in the dispersion of the metallic

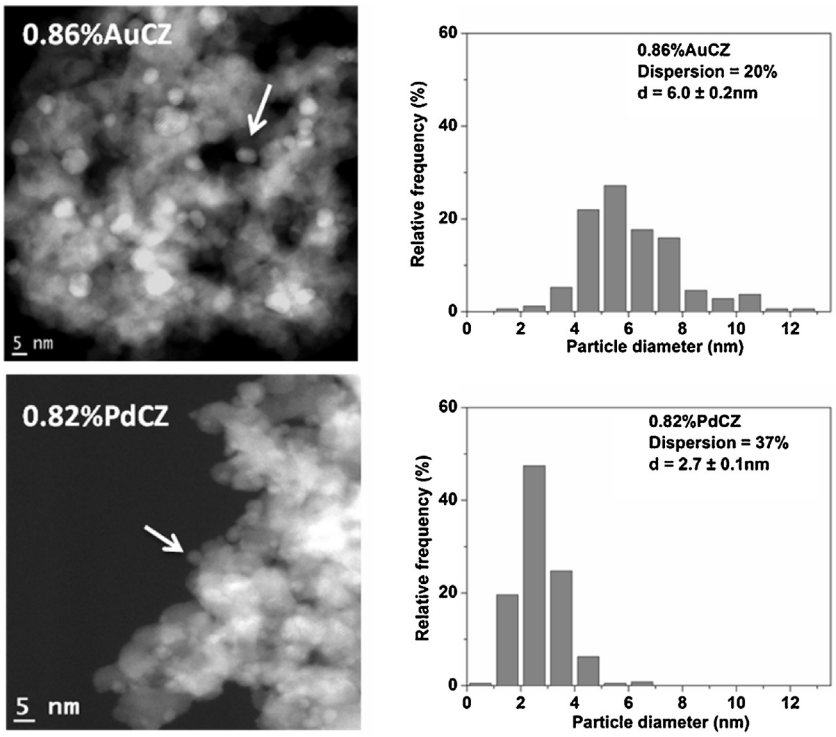

Fig. 4. STEM-HAADF images and particle size distribution of the monometallic catalysts.

phase, which changes from 29 to 37%. It is in any case important to highlight that most metal particles (above 90%) in the bimetallic catalysts are smaller than 5 nm and that the total dispersion is of the same order of that of the monometallic reference catalysts.

Compositional information obtained from STEM-XEDS analysis of individual nanoparticles found on the bimetallic catalysts is also included in Fig. 5. More than 40 individual nanoparticles were analyzed on each sample (Table 3). The graphs in Fig. 5 show both the composition of each analyzed nanoparticle, as a function of their size and the distribution of the whole set of particles among monometallic (Pd or Au) and bimetallic particles. The dashed lines mark the composition corresponding to the Au content determined by ICP-AES, i.e. the macroscopic average Au content (58%).

It is important to highlight that the STEM-XEDS results reveal the presence of both monometallic Au and bimetallic nanoparticles, the former being dominant as shown in Fig. 5. Monometallic Pd nanoparticles represent only a negligible fraction of the analyzed particles in all the catalysts.

The composition of the bimetallic particles falls in the 14–90 mol% Au percentage range, most metal particles being Au-rich. In fact, the composition-size diagrams indicate that only a small fraction of Pd-rich bimetallic particles (Au contents below 50%) can be found on all the catalysts. Thus, the average Au content in the bimetallic particles goes from 64 to 85% (Table 3). Concerning size of the bimetallic particles, the average values range from 3 to 4 nm, the largest value of 3.9 nm detected in the 1.4AuPd-I catalyst and the smallest one of 2.7 nm in 1.4AuPd-O.

From the size and composition of the individual nanoparticles included in Fig. 5 it is possible to make an estimation of the average Au:Pd ratio measured by STEM-XEDS. This calculation leads to the Au:Pd molar ratios included in the last column of Table 3. As expected from the visual inspection of Fig. 5, all the values are much higher than those determined by ICP-AES.

To understand this difference between the macroscopic and nanoscopic analyses it is important to comment on the details of HAADF-STEM imaging in these bimetallic catalysts. Thus, as previously mentioned, the intensity of the contrasts in HAADF-STEM images depends roughly on the square of atomic number of the element (Z^2). Given the large difference in atomic number between oxygen ($Z_O = 16$) and the metallic elements of the support ($Z_{Ce} = 58$ and $Z_{Zr} = 40$), the contrasts from this component of the catalyst are mostly dominated by the metallic cations. If a compositionally averaged, effective, atomic number for the $Ce_{0.62}Zr_{0.38}O_2$ support of 51 is considered, it appears that the HAADF signals generated by the support would be slightly stronger than those produced by the Pd atoms ($Z_{Pd} = 46$) but much weaker than those due to Au ($Z_{Au} = 79$).

For both metals, Au and Pd, the presence of a nanoparticle on top of the surface of a support crystallite should give rise to an increase in the HAADF signal with respect to that corresponding to the neighboring support sites, where no particle is present. This is so because the scattering of the incident electrons at high angles would be additive in the areas where nanoparticle and support overlap. However, since the scattering power of a particle constituted by Au atoms is much higher than that of a pure Pd particle, the number of electrons scattered by a superposition of Au and support would be much higher than that scattered by supported Pd particle. Under these circumstances, for metallic particles of the same size and on crystals of support of the same thickness, the contrast between support and Pd are expected to be smaller than that between support and Au. Note in fact that the Au particles in Fig. 4 appear much brighter than those of Pd.

This difference contributes to an underestimation of the fraction of Pd-rich nanoparticles (especially in the case of very small monometallic Pd particles). In all the catalysts the fraction of smaller particles must be Pd-rich. These Pd particles detected in the HAADF-STEM images and used to calculate the particle size distribution previously shown, but have not been analyzed in proper amount during the STEM-XEDS studies. This bias to Au-rich particles results from the following reasons: firstly, it seems clear that Pd particles are much smaller than Au-containing nanoparticles. This means that for an analytical study representative of the average composition a much higher number of Pd-containing nanoparticles

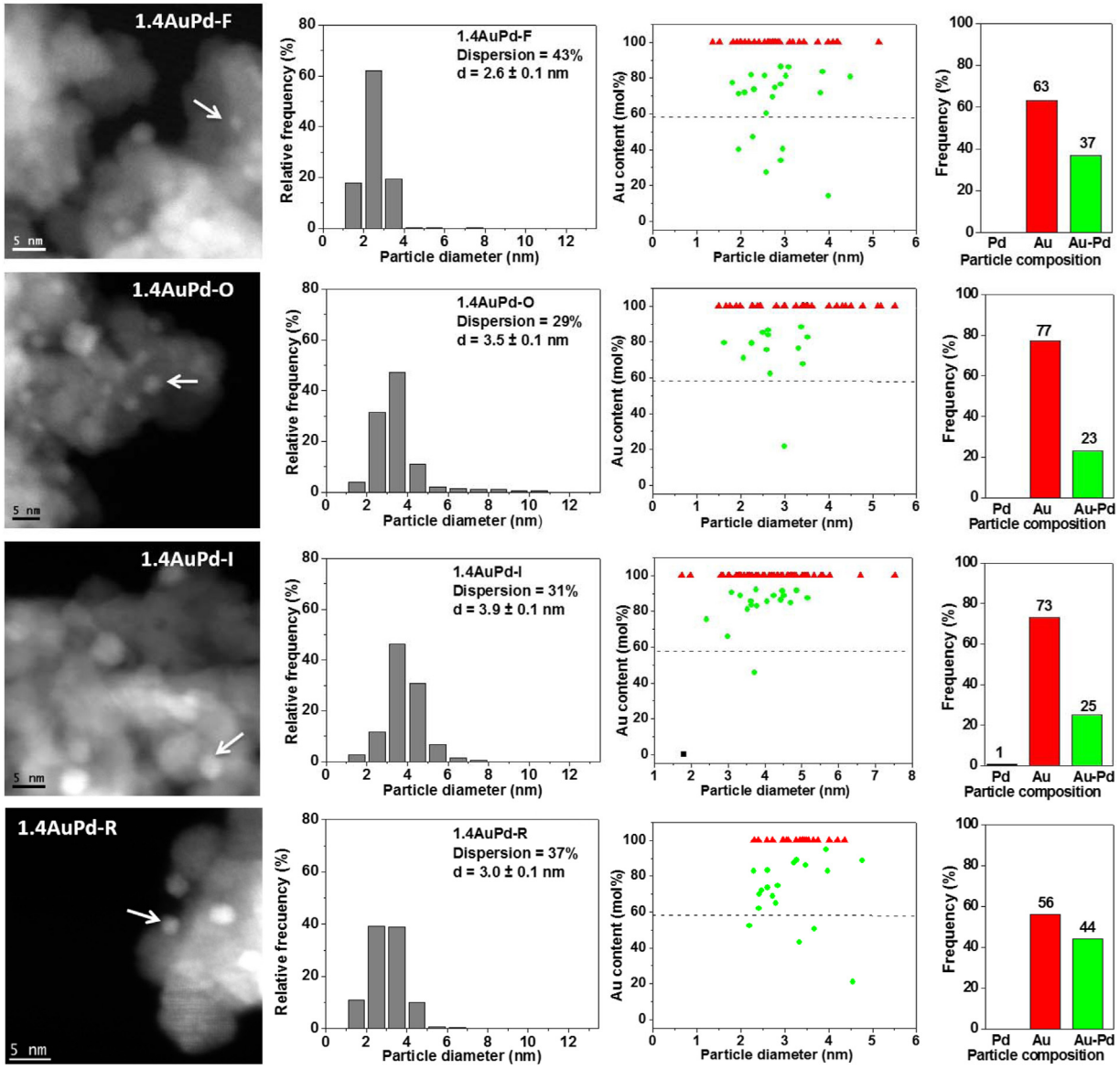

Fig. 5. STEM-HAADF images, particle size distribution, relationship between the particle composition and size and frequencies of Au, Pd and Au-Pd metal particles of bimetallic catalysts determined by EDXS. The dash line is the actual Au:Pd composition obtained by ICP analysis.

Table 3
Estimation of composition of the Au-Pd catalysts derived from XEDS analysis.

Catalyst	Numbers of particles analyzed	Numbers of particles with composition			Mean particle size (nm) [a]			Au content in bimetallic particles[c] (%)	Au content in all particles[d] (%)	Au:Pd molar ratio[d]
		Au	Pd	Au-Pd	Au	Pd[b]	Au-Pd			
1.4AuPd-F	60	38	0	22	2.8	–	2.8	64	86	6.4
1.4AuPd-O	56	43	0	13	3.9	–	2.7	73	98	57
1.4AuPd-I	75	55	1	19	4.2	–	3.9	85	97	30
1.4AuPd-R	43	24	0	19	3.2	–	3.1	69	86	6.2

[a] Average metal particle size as obtained from particles analyzed by XEDS.
[b] Not determined. The average size is not reliable for small numbers of particles.
[c] Atomic percentage of Au content as determined by XEDS considering only bimetallic particles.
[d] Calculated from the data as determined by XEDS with respect to all particles analyzed.

must be analyzed. Secondly, Pd-containing particles show much lower contrasts in HAADF images, increasing difficulties for their selection during the nanoanalytical studies. Thirdly, small particles are also more sensitive to damaging under the electron beam and the signal to noise (S/N) ratio in these particles is smaller. These three factors complicate further their analysis. In other words, a fraction of the Pd particles selected for analysis will render useless spectra due to very poor S/N ratios or beam damage, which in turn increases the ratio of Pd:Au particles to be analyzed.

The solubility of Au in Pd is 0–12 mol% and Pd in Au is 0–31 mol% as reported in the literature [44,45]. For this reason, it is not expected that homogenous bimetallic Au-Pd alloy nanoparticles

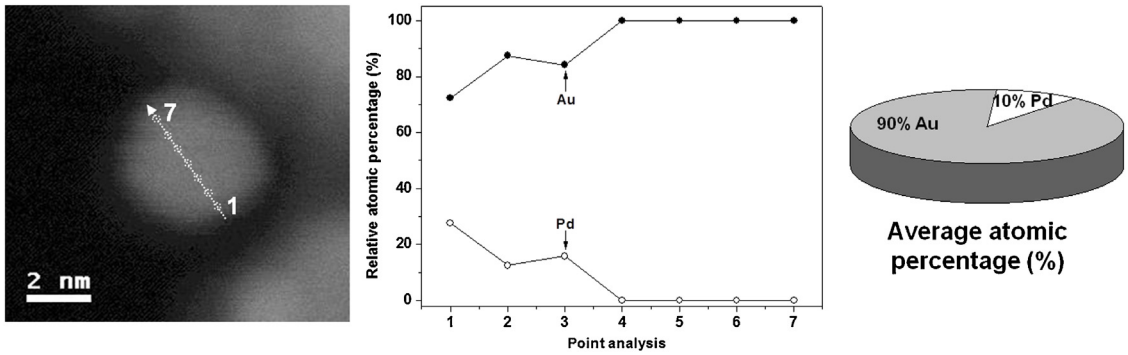

Fig. 6. Line XEDS analysis of a metal particle of 1.4AuPd-R catalyst.

are formed in catalysts like the ones studied here, with a Au:Pd molar ratio of 1.4 and total Au content of 58%. In this respect, Fig. 6 presents the results of a high spatial resolution XEDS analysis performed using a subnanometer, 0.5 nm diameter, electron probe along a linear path through a 4 nm metal particle in the 1.4AuPd-R catalyst. The path starts from one of the surfaces of the particle, crosses though its center and ends on the opposite side of the surface. Concerning the results, it is observed that the Au:Pd composition changes significantly along the path. At the sites close to the lower surface, points 1–3, the Pd content changes from roughly 30% to 15%. In the remaining part of the path, points 4–7, only Au is detected. The average Au content of the whole metal particle is 90 mol% and Pd is only 10 mol%. This result reveals the structural complexity of the bimetallic nanoparticles present in the bimetallic catalysts. As illustrated in this example and in spite of being very small in size, they seem to be constituted by patches, of dimensions smaller than those of the particles themselves, of varying compositions. In other words they seem to be aggregates of nanosized domains of different composition.

Summarizing the STEM results, the sol-immobilization method over the investigated ceria-zirconia support leads to small metal particles, less than 5 nm in diameter of varying composition, very likely due to the limited solubility of Pd in Au. Varying the activation conditions lead to certain changes in the characteristics of the metal nanoparticle system. Nevertheless, all the bimetallic catalysts depict a major fraction of particles with diameters below 5 nm and total dispersion values in the order of the monometallic reference catalysts. Among the metal particles, the fraction of bimetallic type nanoaggregates is in all the catalysts in the 20–45% range. The average composition of these bimetallic nanoparticles is Au-rich, above 60 mol%, in all the catalysts and their average size is close to 3 nm. From the comparison of ICP-AES data and STEM-XEDS results, it appears that a fraction of Pd is related to very small metal nanoparticles.

3.4. XPS results

The chemical composition and the oxidation state of the elements on the surface were investigated by XPS. Quantitative data derived from the XP spectra of the monometallic and bimetallic catalysts, including Au 4f and Pd $3d_{5/2}$ binding energies as well as the corresponding Au:Zr, Pd:Zr and Au:Pd molar ratios, are listed in Table 4. The Au 4f and Pd $3d_{5/2}$ spectra of the catalysts are shown in Figs. 7 and 8. It is commonly accepted that Au $4f_{7/2}$ binding energies in the range 84.1–84.4 eV correspond either to a reduced phase of metallic Au (mostly Au^0) or to large Au nanoparticles [30,33]. Therefore, XPS results suggest that only metallic gold (Au^0) is present in the whole set of catalysts investigated in this paper. Moreover, no change in the Au oxidation state occurs during the treatments under oxidizing, inert or reducing atmospheres. The Pd 3d spectra indicate the formation of two different species: metallic Pd^0 and oxidized $Pd^{\delta+}$ [30]. According to the literature, the binding energies of $Pd^{\delta+}$ species fall in the 336.9–337.6 eV range, whereas metallic Pd^0 species appear about 334.8–336.2 eV [7,9,18,46]. The Pd-containing catalysts in this work present binding energies for $Pd^{\delta+}$ species between 338.1 eV and 338.7 eV, while the metallic Pd^0 species depict signals between 335.9 and 336.2 eV. These values are close to those previously observed on bimetallic Au-Pd nanoparticles supported on ceria-zirconia catalysts prepared by DP of Au followed by impregnation of Pd [30]. The percentage of $Pd^{\delta+}$ in the 0.82%PdCZ catalyst is 18%, which is lower than in all the bimetallic catalysts. Thus, in the fresh bimetallic 1.4AuPd-F catalyst, the total content in oxidized $Pd^{\delta+}$ species is almost doubled, 30% (70% Pd^0). The Pd^0 fraction decreases to ≈55% after the treatment under oxidizing and inert atmospheres at 250 °C. In fact, these two catalysts, 1.4AuPd-O and 1.4AuPd-I, show no difference in the oxidation states of both Au and Pd, in good agreement with the results reported in the literature [42]. As expected, reduction of the 1.4AuPd-O catalyst leads to a higher Pd^0 percentage, this revealing that Pd is reduced during the treatment with H_2 at room temperature. The differences in the oxidation states of Pd suggest that the presence of Au promotes the oxidation of Pd.

As mentioned in previous studies [12,30], zirconium is homogeneously distributed in the mixed ceria-zirconia oxide support used in this work. Therefore, Au:Zr and Pd:Zr molar ratios provide reliable information about relative amounts of Au and Pd atoms available on the surface of the catalysts. The analysis depths of Au and Pd using XPS have been calculated using data available from the Refs. [47,48]. Thus, for the Au 4f signal, the analysis depth is between 5.4 and 5.8 nm, whereas that of Pd 3d reaches only between 4.6 and 5.0 nm. These values have to be taken into account to interpret properly the observed Au:Zr and Pd:Zr ratios in the different catalysts.

As discussed in the STEM results section, the average metal particle size in the 0.86%AuCZ catalyst was 6 nm but a small percentage of the particles present diameters above 11 nm, which is just about twice the maximum analysis depth. For these Au particles only the atoms at distances from the surface shorter than 5.8 nm would be detected by XPS. In other words, all the atoms at the core of these very big Au particles would not be detected by XPS. On the other hand, all the Pd particles in the 0.82%PdCZ catalyst are smaller than 10 nm (Fig. 4). Therefore, all the Pd atoms in this catalyst would be within the XPS analysis range.

If the atomic weights of Au and Pd are considered, the moles of Au in the 0.86%AuCZ catalyst should be roughly half those of Pd in 0.82%PdCZ. If this factor is taken into account jointly with the presence of a fraction of very large particles in the case of the monometallic gold catalysts, the higher value of the Pd:Zr ratio in the 0.82%PdCZ catalyst (0.42), as compared to that of Au:Zr in the 0.86%AuCZ (0.06), can be understood. The very large difference

Table 4
Quantitative XPS data from the monometallic and bimetallic catalysts.

Catalyst	Ce^{3+} in total amount of Ce %)	Au $4f_{7/2}$		Pd $3d_{5/2}$				Molar ratios				
		Au^0 (%)	Binding energy of Au^0 (eV)	Pd^0(%)	Binding energy of Pd^0 (eV)	$Pd^{\delta+}$(%)	Binding energy of $Pd^{\delta+}$ (eV)	Zr:Ce	Au:Zr	Pd:Zr	Au:Pd	Au content (mol%)
0.86%AuCZ	25	100	84.2	–	–	–	–	0.40	0.06	–	–	100
1.4AuPd-F	22	100	84.2	70	336.1	30	338.2	0.40	0.13	0.09	1.40	58
1.4AuPd-O	21	100	84.2	55	336.0	45	338.1	0.40	0.09	0.06	1.49	60
1.4AuPd-I	19	100	84.3	54	336.2	46	338.1	0.44	0.07	0.07	1.04	51
1.4AuPd-R	20	100	84.3	59	336.0	41	338.7	0.50	0.09	0.05	1.71	63
0.82%PdCZ	14	–	–	82	335.9	18	338.1	0.44	–	0.42	–	0

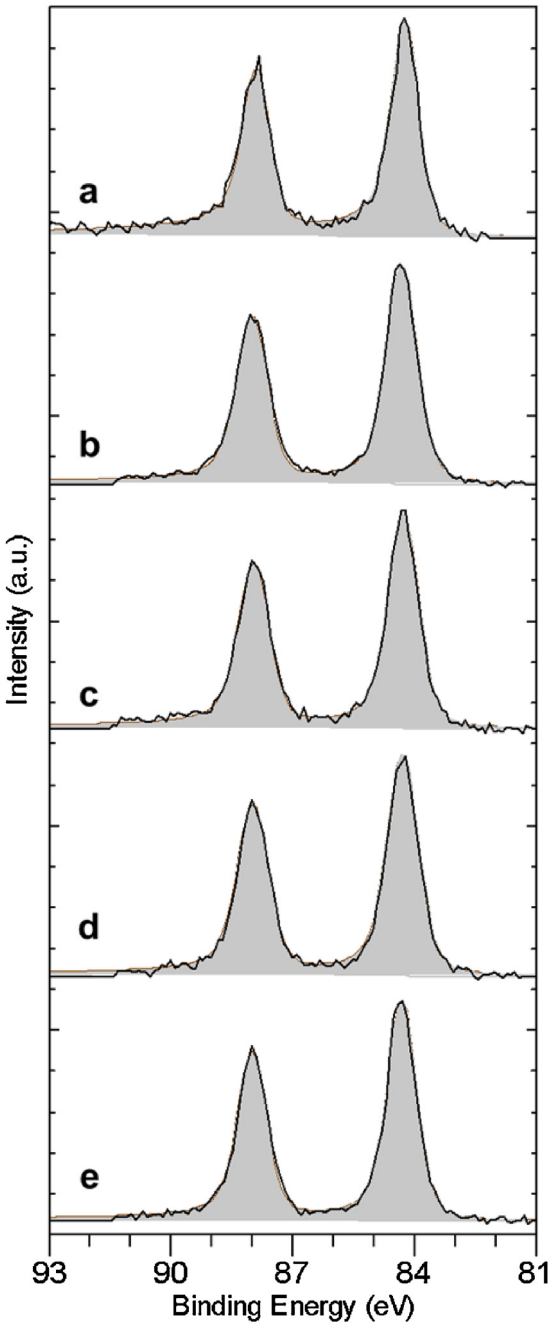

Fig. 7. XPS high resolution spectra corresponding to Au 4f for samples listed in Table 4: (a) 0.86%AuCZ, (b) 1.4AuPd-F, (c) 1.4AuPd-O, (d) 1.4AuPd-I, and (e) 1.4AuPd-R.

between these two parameters does in any case reveal that the availability of metal atoms on the surface of the monometallic Pd catalyst is much higher than in the monometallic Au counterpart.

In the bimetallic catalysts, all the metal particles are smaller than 10 nm in diameter as seen in Fig. 5. Therefore, XP spectra should account in this case for all the metal atoms present in these catalysts. The Au:Zr and Pd:Zr molar ratios in the 1.4AuPd-F catalyst are higher than those corresponding to the 1.4AuPd-O and 1.4AuPd-I catalysts. This indicates that at least some sintering of the metal particles occurs during the thermal treatments (Table 4), which is in good agreement with the STEM results. The Au:Zr and Pd:Zr ratios decrease in the 1.4AuPd-O catalyst with respect to the values in 1.4AuPd-F catalyst, by a similar factor, this suggesting that sintering affects homogeneously to both metal components. Thus the Au:Pd molar ratio in the 1.4AuPd-O catalyst is 1.4, which is quite close to the value of the 1.4AuPd-F (1.5). In contrast, the Au:Zr ratio decreases more than the Pd:Zr ratio after the activation treatment under inert atmosphere, this leading to a lower Au:Pd molar ratio (1.04). The decrease of the Au:Pd molar ratio in the 1.4AuPd-I catalyst indicates that sintering affects more severely to Au than Pd. Hutchings et al. showed that the Pd:Au ratios increased with calcination temperature on an activated carbon support, whereas it maintained almost constant on TiO_2 [43], this difference being very likely due to the intrinsic surface properties of both supports. The Pd:Zr ratio in the 1.4AuPd-R catalyst is slightly lower than that observed on its precursor (1.4AuPd-O catalyst), resulting in a small increase in the Au:Pd ratio.

Concerning the percentages of Ce^{3+} in the monometallic and bimetallic catalysts, XPS indicate that, at the level of the surface, they are quite similar, around 20%. It is important to indicate that all the catalysts were analyzed after exposure to air. Since these catalysts were not submitted to further pretreatment before measuring their catalytic activity, it is not expected that differences in the reduction degree of ceria can contribute to differences in catalytic activity for benzyl alcohol oxidation.

Finally, the presence of residual PVP on the samples was followed by means of the presence of N 1s signal in the survey spectra of the samples. As suggested previously in the catalytic activity Section 3.2, some of the investigated catalysts could remain some PVP moieties on their surfaces, which could be attributed to the low catalytic activity observed for 0.82%PdCZ, 1.4AuPd-F and 1.4AuPd-R samples. Since all the investigated samples were analyzed by XPS without degassing or cleaning their surface, the presence of PVP could be masked by the signals corresponding to adventitious carbon, present in all the samples. For this reason, the N 1s signal was selected, as it is an element that is characteristic of the PVP polymer, and should be absent from the surfaces of the clean samples. Fig. S1 shows the region around the N 1s signal for all the catalysts, as well as a table (shown as an inset) with the calculated N 1s/Zr 3d atomic ratios. Nitrogen, and thus some PVP residues, could only be detected in the fresh bimetallic catalyst, and in much

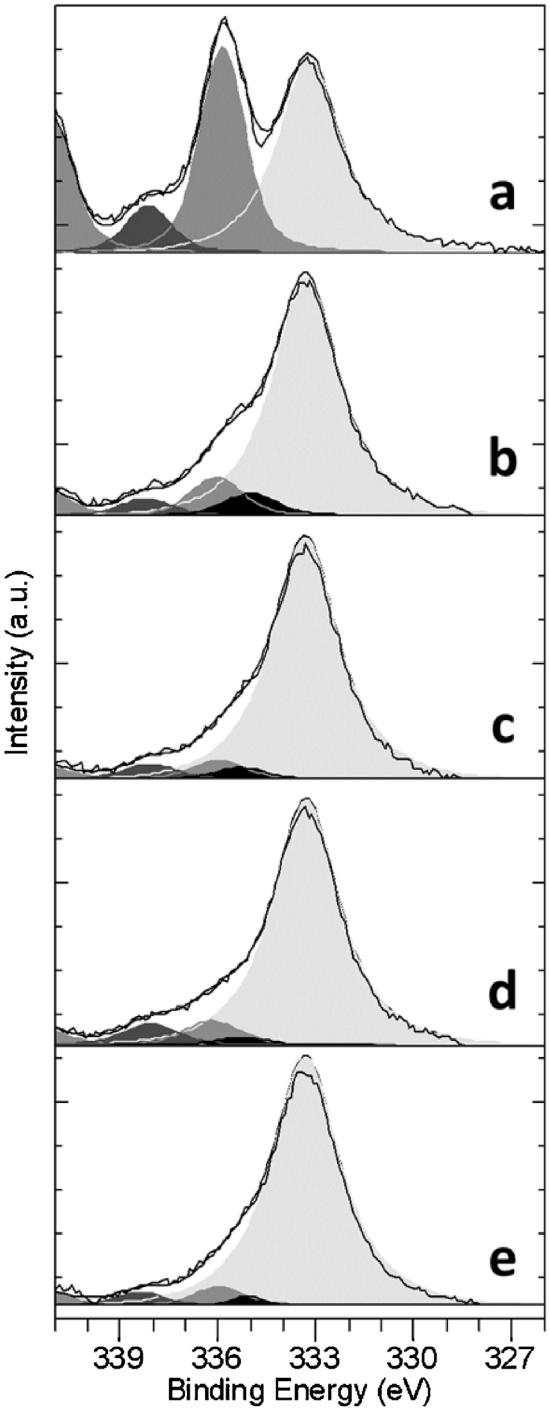

Fig. 8. XPS high resolution spectra for samples listed in Table 4, corresponding to Zr $3p_{3/2}$ (light gray), Pd $3d_{5/2}$ (medium and dark gray corresponding to Pd^0 and $Pd^{\delta+}$, respectively) and Au $4d_{5/2}$ (black): (a) 0.82%PdCZ, (b) 1.4AuPd-F, (c) 1.4AuPd-O, (d) 1.4AuPd-I, and (e) 1.4AuPd-R.

lower amounts in the reduced catalyst and in the monometallic Pd sample.

4. Discussion

The particle size distribution, the compositional homogeneity and the morphology of metal particles are parameters expected to affect the catalytic activities of bimetallic Au-Pd samples. Actually, Hutchings and other researchers have intended to correlate the catalytic activity with the morphology of bimetallic Au-Pd catalysts [4]. They reported that a Au-rich core surrounded by a Pd-rich shell structure improved the overall selectivity and influenced also the catalytic activities [4]. Nevertheless, most articles showed only a single TEM image of a single metal particle to illustrate the morphology of bimetallic Au-Pd catalyst. Few works reported comprehensive chemical composition studies of a very large set of individual metal particles correlating it with metal particle size [12]. As the STEM results presented in this paper reveal (Fig. 5), even for the most active catalyst (1.4AuPd-O), only 23% of the metal particles are bimetallic particles whereas the rest are monometallic ones. The reference monometallic 0.86%AuCZ catalyst, with average particle size of 6 nm, shows a very limited activity (Fig. 3). Likewise, the second monometallic 2.5%AuCZ catalyst, with average particle size of 1.7 nm, also exhibits a very low activity for this reaction (Fig. 3). This indicates that neither large Au particles around 6 nm in diameter, nor smaller Au particles around 2 nm, are active for benzyl alcohol oxidation. The intrinsic activity of the monometallic 0.82%PdCZ catalyst is also moderate.

All the bimetallic Au-Pd catalysts contain a major fraction (roughly between 55–80%) of Au nanoparticles and a minor fraction of bimetallic Au-Pd particles (20–45%). However, as discussed in STEM result section, the fraction of monometallic Pd and Pd-containing bimetallic particles has been underestimated due to the difficulty of visualization of small Pd containing particles using STEM-HAADF technique. Direct correlation between the catalytic activity and fraction of different types of metal particles cannot be easily made.

The lower activity of the fresh bimetallic catalyst, which contains a higher fraction of bimetallic particles of roughly the same average size as those in the oxidized 1.4AuPd-O catalyst, is possibly linked to the presence of PVP residues which were not removed during the washing and drying procedures, as deduced from TPO results of 1.4AuPd-F sample, and from the XP spectra shown in the supporting information (Fig. S1). Oxidizing and inert atmospheres at 250 °C are able to remove the PVP on the surface of the catalyst and enhance their catalytic activity. Hutchings et al. reported similar results on bimetallic Au-Pd supported on activated carbon [42], indicating that a calcination at 250 °C in air led to a catalyst showing higher activity than the one dried at 120 °C, which still contained PVP residues.

It is also true that the 1.4AuPd-F catalyst is the one showing the lowest fraction of oxidized $Pd^{\delta+}$ species, 30% against the 40–46% observed in the other catalysts. In any case the separate influence of PVP contamination and electronic state of Pd cannot be disentangled from our data.

Regarding specifically with the role of the oxidation state of the two metals, XPS results clearly indicate that, in all the catalysts, metallic Pd^0 and oxidized $Pd^{\delta+}$ species coexist, whereas gold is only present as metallic Au^0. Though the separate influence of Pd oxidation state cannot be very precisely established, the comparison of the bimetallic catalysts free of PVP residues point out the importance of the coexistence of reduced Au and oxidized Pd species in their activity in benzyl alcohol oxidation. Thus, in the case of 1.4AuPd-O and 1.4AuPd-R catalysts which present bimetallic nanoparticles of similar average size (3 nm) and similar composition (about 70 mol% Au), the former (containing 45% oxidized $Pd^{\delta+}$) is more active than the later (containing 41% $Pd^{\delta+}$). The comparison with 1.4AuPd-I is more complicated, since for this catalyst the fraction of oxidized $Pd^{\delta+}$ is close to that of 1.4AuPd-O but there are significant differences between them in terms of both average bimetallic particle size and composition.

Regarding catalytic activity, the results provide clues about the occurrence of synergy between the two metals, Au and Pd when dispersed on ceria-zirconia mixed oxides in the form of very small nanoparticles. The actual catalytic activity of the bimetallic catalyst depends on the size distribution and composition of the bimetallic nanoparticles, as well as on the average electronic state of Pd. A much more detailed experimentation would be required to neatly separate the contributions of each of these factors. Solving this puzzling question would require preparing series of bimetallic catalysts in which each factor could be independently varied, which is in fact a rather complex goal to achieve and clearly out of the scope of the first insight into the behavior of highly dispersed Au-Pd bimetallic catalysts supported on ceria-zirconia mixed oxides pursued in this paper.

5. Conclusions

Bimetallic Au-Pd catalysts supported on a $Ce_{0.62}Zr_{0.38}O_2$ mixed oxide, with a Au:Pd molar ratio of 1.4, have been synthesized by sol-immobilization method. Different catalysts were obtained by modifying the redox nature (oxidizing, inert and reducing) of the pretreatment atmosphere during their activation. A synergic effect between Au and Pd has been observed for oxidation of benzyl alcohol on these catalysts. A benzyl alcohol conversion of 97% and a selectivity toward benzaldehyde of 96% is achieved over the oxidized 1.4AuPd-O catalyst, which is the catalyst depicting the best performance.

A combined STEM-HAADF and STEM-XEDS studies reveal that in all the catalysts most metal nanoparticles are very small, below 5 nm in diameter. A fraction of these nanoparticles ranging roughly from 20 to 45% are bimetallic Au-Pd nanoaggregates in which small, subnanometer sized, Au and Pd rich domains are merged together into single particles. In the specific case of the 1.4AuPd-O catalyst, only 23% of the metal particles are bimetallic, while the rest are monometallic particles. This small fraction of bimetallic Au-Pd particles is responsible of the observed large enhancement of the catalytic activity for this reaction.

The thermal treatments under oxidative and inert atmospheres remove the protecting agent PVP, which results in an improvement of the catalytic activity of the fresh 1.4AuPd-F catalyst, even though the metal particle size slightly increase after the thermal treatments. The comparison of the catalytic activity of the activated catalysts with their structure, as revealed by XRD, STEM and XPS, suggests that the catalytic activity is influenced by the size and composition of the bimetallic aggregates. Moreover, the oxidation state of Pd in the catalyst also plays a major role in activity, the two most active catalyst showing higher percentages of $Pd^{\delta+}$ species.

Finally, it is also important to highlight that a comparison of the results presented in this paper with previous data in the literature using activated carbon or carbon nanotubes as supports, reveal that ceria-zirconia improves the catalytic performance of the Au-Pd bimetallics, pointing out to an influence of the supporting material on benzyl alcohol oxidation.

Acknowledgements

This work has been supported by the Ministry of Science and Innovation of Spain/FEDER Program of the EU (MAT 2013-40823-R), CSD2009-00013 and Junta de Andalucía Project FQM-3994. J. J. Delgado and X. Chen thank the "Ramón y Cajal" Program from Ministry of Science and Innovation of Spain. Huiyan Pan acknowledges the PhD fellowship from Chinese Scholarship Council.

Appendix A. Supplementary data

Supplementary data associated with this article can be found, in the online version, at http://dx.doi.org/10.1016/j.apcata.2016.07.013.

References

[1] J.A.B. Satrio, L.K. Doraiswamy, Chem. Eng. J. 82 (2001) 43.
[2] D. Wang, A. Villa, P. Spontoni, D.S. Su, L. Prati, Chem. Eur. J. 16 (2010) 10007.
[3] N. Dimitratos, A. Villa, D. Wang, F. Porta, D. Su, L. Prati, J. Catal. 244 (2006) 113.
[4] D.I. Enache, J.K. Edwards, P. Landon, B. Solsona-Espriu, A.F. Carley, A.A. Herzing, M. Watanabe, C.J. Kiely, D.W. Knight, G.J. Hutchings, Science 311 (2006) 362.
[5] J. Feng, C. Ma, P.J. Miedziak, J.K. Edwards, G.L. Brett, D. Li, Y. Du, D.J. Morgan, G.J. Hutchings, Dalton Trans. 42 (2013) 14498.
[6] A. Villa, N. Janjic, P. Spontoni, D. Wang, D.S. Su, L. Prati, Appl. Catal. A 364 (2009) 221.
[7] J. Pritchard, L. Kesavan, M. Piccinini, Q. He, R. Tiruvalam, N. Dimitratos, J.A. Lopez-Sanchez, A.F. Carley, J.K. Edwards, C.J. Kiely, G.J. Hutchings, Langmuir 26 (2010) 16568.
[8] D.I. Enache, D. Barker, J.K. Edwards, S.H. Taylor, D.W. Knight, A.F. Carley, G.J. Hutchings, Catal. Today 122 (2007) 407.
[9] S. Marx, A. Baiker, J. Phys. Chem. C 113 (2009) 6191.
[10] P. Miedziak, M. Sankar, N. Dimitratos, J.A. Lopez-Sanchez, A.F. Carley, D.W. Knight, S.H. Taylor, C.J. Kiely, G.J. Hutchings, Catal. Today 164 (2011) 315.
[11] G. Zhan, Y. Hong, V.T. Mbah, J. Huang, A.-R. Ibrahim, M. Du, Q. Li, Appl. Catal. A 439–440 (2012) 179.
[12] C.M. Olmos, L.E. Chinchilla, E.G. Rodrigues, J.J. Delgado, A.B. Hungría, G. Blanco, M.F.R. Pereira, J.J. Órfão, J.J. Calvino, X. Chen, Appl. Catal. B 197 (2016) 222.
[13] L.E. Chinchilla, C.M. Olmos, M. Kurttepeli, S. Bals, G. Van Tendeloo, A. Villa, L. Prati, G. Blanco, J.J. Calvino, X. Chen, A.B. Hungría, Part. Part. Syst. Charact. (2016), http://dx.doi.org/10.1002/ppsc.201600057.
[14] H. Zhang, Y. Xie, Z. Sun, R. Tao, C. Huang, Y. Zhao, Z. Liu, Langmuir 27 (2011) 1152.
[15] Z. Zhang, Y. Wang, X. Li, W.-L. Dai, Chin. J. Catal. 35 (2014) 1846.
[16] P.J. Miedziak, Z. Tang, T.E. Davies, D.I. Enache, J.K. Bartley, A.F. Carley, A.A. Herzing, C.J. Kiely, S.H. Taylor, G.J. Hutchings, J. Mater, Chem 19 (2009) 8619.
[17] W. Cui, Q. Xiao, S. Sarina, W. Ao, M. Xie, H. Zhu, Z. Bao, Catal. Today 235 (2014) 152.
[18] Y. Chen, H. Wang, C.-J. Liu, Z. Zeng, H. Zhang, C. Zhou, X. Jia, Y. Yang, J. Catal. 289 (2012) 105.
[19] G.J. Hutchings, C.J. Kiely, Accounts Chem. Res. 46 (2013) 1759.
[20] L. Prati, A. Villa, C.E. Chan-Thaw, R. Arrigo, D. Wang, D.S. Su, Faraday Discuss. 152 (2011) 353.
[21] G.J. Hutchings, Catal. Today 238 (2014) 69.
[22] X. Yang, C. Huang, Z. Fu, H. Song, S. Liao, Y. Su, L. Du, X. Li, Appl. Catal. B 140–141 (2013) 419.
[23] Y. Chen, H. Lim, Q. Tang, Y. Gao, T. Sun, Q. Yan, Y. Yang, Appl. Catal. A 380 (2010) 55.
[24] C.Y. Ma, B.J. Dou, J.J. Li, J. Cheng, Q. Hu, Z.P. Hao, S.Z. Qiao, Appl. Catal. B 92 (2009) 202.
[25] A. Villa, D. Wang, D.S. Su, L. Prati, Catal. Sci. Technol. 5 (2015) 55.
[26] A. Abad, P. Concepción, A. Corma, H. García (Eds.), Angew. Chem. Int. 44 (2005) 4066.
[27] G. Vlaic, R. Di Monte, P. Fornasiero, E. Fonda, J. Kašpar, M. Graziani, J. Catal. 182 (1999) 378.
[28] B.M. Reddy, A. Khan, Catal. Surv. Asia 9 (2005) 155.
[29] K. Narasimharao, T.T. Ali, Catal. Lett. 143 (2013) 1074.
[30] C.M. Olmos, L.E. Chinchilla, J.J. Delgado, A.B. Hungría, G. Blanco, J.J. Calvino, X. Chen, Catal. Lett. 146 (2016) 144.
[31] L.E. Chinchilla, C.M. Olmos, A. Villa, A. Carlsson, L. Prati, X. Chen, G. Blanco, J.J. Calvino, A.B. Hungría, Catal. Today 253 (2015) 178.
[32] M. López-Haro, J.J. Delgado, J.M. Cies, E. del Rio, S. Bernal, R. Burch, M.A. Cauqui, S. Trasobares, J.A. Pérez-Omil, P. Bayle-Guillemaud, J.J. Calvino (Eds.), Angew. Chem. Int. 49 (2010) 1981.
[33] J.M. Cies, E. del rio, M. Lopez-Haro, J.J. Delgado, G. Blanco, S. Collins, J.J. Calvino, S. Bernal (Eds.), Angew. Chem. Int. 49 (2010) 9744.
[34] M. Haruta, N. Yamada, T. Kobayashi, S. Iijima, J. Catal. 115 (1989) 301.
[35] E.D. Park, J.S. Lee, J. Catal. 186 (1999) 1.
[36] T. Mallat, A. Baiker, Chem. Rev. 104 (2004) 3037.
[37] Q. He, P.J. Miedziak, L. Kesavan, N. Dimitratos, M. Sankar, J.A. Lopez-Sanchez, M.M. Forde, J.K. Edwards, D.W. Knight, S.H. Taylor, C.J. Kiely, G.J. Hutchings, Faraday Discuss. 162 (2013) 365.
[38] A. Villa, D. Wang, N. Dimitratos, D. Su, V. Trevisan, L. Prati, Catal. Today 150 (2010) 8.
[39] A. Savara, C.E. Chan-Thaw, I. Rossetti, A. Villa, L. Prati, ChemCatChem 6 (2014) 3464.

[40] S. Meenakshisundaram, E. Nowicka, P.J. Miedziak, G.L. Brett, R.L. Jenkins, N. Dimitratos, S.H. Taylor, D.W. Knight, D. Bethell, G.J. Hutchings, Faraday Discuss. 145 (2010) 341.
[41] C. Keresszegi, D. Ferri, T. Mallat, A. Baiker, J. Phys. Chem. B 109 (2005) 958.
[42] J. Pritchard, M. Piccinini, R. Tiruvalam, Q. He, N. Dimitratos, J.A. Lopez-Sanchez, D.J. Morgan, A.F. Carley, J.K. Edwards, C.J. Kiely, G.J. Hutchings, Catal. Sci. Technol. 3 (2013) 308.
[43] A.A. Herzing, A.F. Carley, J.K. Edwards, G.J. Hutchings, C.J. Kiely, Chem. Mat. 20 (2008) 1492.
[44] A. Maeland, T.B. Flanagan, Can. J. Phys. 42 (1964) 2364.
[45] J. Xu, T. White, P. Li, C. He, J. Yu, W. Yuan, Y.-F. Han, J. Am. Chem. Soc. 132 (2010) 10398.
[46] K. Qian, W. Huang, Catal. Today 164 (2011) 320.
[47] C. Powell, A. Jablonski, NIST Electron Inelastic- Mean-Free-path Database, Version 1.2, SRD 71, National Institute of Standards and Technology, Gaithersburg MD, 2010.
[48] W.H. Gries, Surf. Interface Anal. 24 (1996) 38.